Food Hydrocolloids 184 (2027) 113280

Contents lists available at ScienceDirect

Food Hydrocolloids

journal homepage: www.elsevier.com/locate/foodhyd

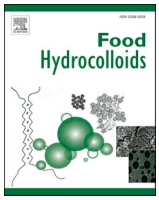

Complex structured meat analogues via hybrid extrusion printing by incorporation of oil-containing ionically gelling alginate binders

Laurids Pernice [a,*], Luca Dennig [a], Birgit Hetzer [b], Eric Gottwald [c], Ulrike S. van der Schaaf [a], Nico Leister [a]

[a] Karlsruhe Institute of Technology (KIT), Institute of Process Engineering in Life Sciences – Food Process Engineering, Karlsruhe, Germany
[b] Max Rubner-Institut (MRI), Federal Research Institute of Nutrition and Food, Innovation Centre for Food and Process Technologies, Karlsruhe, Germany
[c] Karlsruhe Institute of Technology (KIT), Institute of Functional Interfaces, Karlsruhe, Germany

ARTICLE INFO

Keywords:
Meat alternatives
High-moisture extrusion
Food printing
Soy protein isolate
Sustainable food systems
Co-extrusion
Structured food
Protein texturization

ABSTRACT

Over recent decades, consumer demand has driven meat analogue development. While alternatives to minced meat products (e.g. patties and sausages) are widely available, replication of whole-cut meat products remains challenging due to their complex structure and composition including muscle fiber bundles as well as fat-rich connective tissue, which largely determine appearance, flavor, and texture. In this study, the applicability of novel a bi-stream breaker plate system in high-moisture twin-screw extrusion was investigated for the production of structurally complex, multi-phase meat analogues. An inline external gelation approach was employed using $CaCl_2$-containing protein-mass to solidify alginate-based binders. Protein-mass temperature (100, 120, 140 °C), binder flow fraction relative to the extrudate (0, 4, 7, 13 wt%), and dispersed oil content in the binder (0, 10, 20 wt%) were varied independently. Samples were optically assessed (tearing analysis, Cryo-SEM, CLSM) and mechanical testing (texture profile analysis, cutting tests). Additionally, the rheological behavior of the protein-mass was characterized in dependence of temperature and $CaCl_2$ concentration. Results show predominantly homogeneous binder distributions up to protein-mass temperatures of 120 °C. Increasing binder fraction did not affect its distribution across the extrudate width. Mechanical analysis revealed a continuous decrease in chewiness (up to 48 % reduction), while anisotropy increased by 40 % upon initial binder incorporation. Increasing the dispersed oil fraction reduced chewiness (up to 17 % reduction). Microstructural analysis confirmed that binder layers spatially separated protein strands, thereby inhibiting their recombination. This scalable extrusion-based process thus represents a promising alternative to 3D-printing, combining protein-rich and oil-rich layers into complex structures.

1. Introduction

In recent years, significant progress has been made in the development of meat product substitutes. As noted by McClements & Grossmann (2021), the industry has successfully mastered the production of formed products, such as patties, nuggets, and sausages. However, the development of whole-muscle meat products remains considerably more challenging (McClements & Grossmann, 2021; Younis et al., 2023).

Among current processing technologies, extrusion has become the dominant industrial method for producing structured plant proteins (Vallikkadan et al., 2023). In particular, high-moisture extrusion enables the formation of anisotropic protein structures. Several hypotheses have been proposed to explain structure formation during this process. These include flow-induced alignment of protein molecules and aggregates under thermomechanical treatment, phase separation phenomena within the protein-mass, as well as gel fracture and subsequent healing mechanisms occurring under shear. In addition, water migration processes such as syneresis during cooling are thought to contribute to the stabilization of the final anisotropic structure (van der Sman & van der Goot, 2023).

However, despite its effectiveness in generating fibrous structures, extrusion-based products often fail to fully replicate the textural properties of real meat, with Mateen et al. highlighting innovative die design as a potential strategy to address this limitation (Mateen et al., 2023). Sha and Xiong noted the limiting factor in replicating the complex hierarchical organization of animal muscle, as well as the associated

* Corresponding author. Karlsruhe Institute of Technology (KIT), Institute of Process Engineering in Life Sciences, Food Process Engineering, Karlsruhe, Germany.
E-mail address: laurids.pernice@kit.edu (L. Pernice).

https://doi.org/10.1016/j.foodhyd.2026.113280
Received 1 July 2026; Received in revised form 12 August 2026; Accepted 17 August 2026
Available online 18 August 2026
0268-005X/© 2026 The Authors. Published by Elsevier Ltd. This is an open access article under the CC BY license (http://creativecommons.org/licenses/by/4.0/).

sensory properties, including the characteristic juiciness perceived during consumption (Sha & Xiong, 2020). Dekkers et al. highlight bottom-up approaches as having a higher potential to resemble the hierarchical meat structure, but also point towards top-down strategies (such as extrusion) in terms of robustness, scalability, and resource efficiency (Dekkers et al., 2018). To combine both objectives, recent research has increasingly focused on the controlled formation of hierarchical structures during extrusion-based processing (Pernice et al., 2025; Zheng et al., 2024). Building on this concept, Pernice et al. introduced Hybrid Extrusion Printing (HEP), a co-extrusion-based process utilizing a novel bi-stream breaker plate system designed for the continuous production of multi-phase meat analogues (Pernice et al. (manuscript under review)). In this configuration, the protein-mass is divided into individual streams, while a gelatin-based binder is simultaneously delivered through dedicated channels between the protein streams. This setup not only replicates the length scales of muscle fiber bundles but also emulates the functional role of the intermediate connective tissue layer. By preventing recombination of adjacent protein strands downstream of the breaker plate, the binder promotes the formation of a pronounced anisotropic structure while enabling controlled release of liquids. HEP therefore offers a combination of advantages. It maintains the scalability and throughput of high-moisture extrusion, while simultaneously enabling the generation of complex, multi-phase structures approaching the spatial precision of 3D printing, thereby enhancing both structural anisotropy and liquid release in the resulting meat analogues.

While Pernice et al. demonstrated the potential of HEP technology for meat analogue production using gelatin as a thermally gelling binder (Pernice et al. (manuscript under review)), to the best of our knowledge, no study has yet investigated the application of ionically gelling agents as a binder within a co-extrusion setup for meat analogues.

Ionically gelling agents such as alginates and pectins are widely used in food engineering, representing a particularly relevant class of hydrocolloids in the context of vegan nutrition. When applied as binders, these systems are expected to provide improved process stability, as their gelation mechanism is largely independent of temperature gradients. This decoupling is particularly relevant in extrusion processing, where temperature strongly governs texturization of proteins. Moreover, ionically gelling binders may also contribute to enhanced cooking stability, which can be attributed to the same temperature-decoupled gelation mechanism.

The present work therefore aims to explore how HEP can be used as a novel continuous processing route to generate, for the first time, bi- and multiphase extrudates consisting of spatially separated protein-rich domains and ionically gelled alginate-based domains. To this end, soy protein isolate (SPI) is combined with the divalent cation Ca^{2+} to induce in-process ionic gelation of an alginate-based binder.

To access processing characteristics, pressure during extrusion, rheological properties of the protein-mass as well as optical investigation of the spatial distribution of binder between the protein strands was used. Product structure is characterized at both the macroscopic and microscopic levels using optical methods, including tear images, confocal laser scanning microscopy (CLSM), and cryogenic scanning electron microscopy (Cryo-SEM). Furthermore, the mechanical properties of the extrudates are investigated using texture profile analysis (TPA) to determine chewiness and cutting tests to assess mechanical anisotropy.

Guiding this study, we hypothesize that ionically gelling alginate-based binders can be uniformly distributed between the protein strands and subsequently stabilized via external gelation through diffusion of calcium ions from the protein strands. We further propose that increasing the binder flow fraction reduces the chewiness of the extrudates, while the initial incorporation of the binder enhances structural anisotropy. Notably, further increases in the binder flow fraction are expected to have only a minor effect on anisotropy, as the protein strands are already spatially separated. Finally, the addition of oil as a dispersed phase to the alginate-based binder, stabilized with Tween 20, is expected to act as an inactive filler, reducing chewiness while having little impact on the overall anisotropic structure.

1.1. Background regarding the alginate gelation mechanism

Gelation mechanisms may be classified as either physical or chemical in nature, with ionic interactions responsible for alginate gelation being categorized as a form of physical crosslinking (Hecht & Srebnik, 2016).

Depending on its source, alginate consists of homopolymeric blocks of α-L-guluronate (G blocks) or β-D-mannuronate (M blocks), as well as heteropolymeric alternating blocks (MG blocks), with the relative proportions of these blocks varying between sources. G blocks are primarily responsible for ionic gelation via the egg-box model, first proposed by Grant (Grant et al., 1973). This process involves the incorporation of multivalent cations, such as calcium ions, and is facilitated by the stiff, buckled conformation of the G-block chains (Draget & Taylor, 2011).

The alginate sol/gel transition per se is considered temperature-independent (Draget et al., 1997). However, the diffusion coefficient in solutions is proportional to temperature (Pilling & Seakins, 2007). Consistently, Jeong et al. demonstrated that lowering the gelation temperature reduces the diffusion rate of calcium ions, further affecting the gelation kinetics (Jeong et al., 2020). With respect to the extrusion trials involving inline gelation of alginate upon contact with a hot protein-mass, this may contribute to an enhanced gelation process compared to gelation at room temperature.

2. Materials and methods

2.1. Materials

SPI (90 wt% protein content, dry basis; moisture < 6 %; pH (5 % slurry) = 6.9–7.4; fat < 1 %; ash < 5 % according to the manufacturer) was obtained from Solae LLC (St. Louis, MO, USA) and used as the protein source. Sodium alginate (Carl Roth GmbH + Co. KG, Karlsruhe, Germany; molecular weight 300–350 kDa, mannuronic acid 50–60 %, guluronic acid 40–50 %) served as the ionically gelling hydrocolloid for the binder (viscosity data shown in Fig. A18). Tap water from Stadtwerke Karlsruhe (Karlsruhe, Germany; 3.2 mmol/l $CaCO_3$) was used throughout all experiments. Oil-in-water emulsions were prepared using canola oil (Brökelmann + Co. – Ölmühle GmbH + Co., Hamm, Germany) and Tween 20 (Carl Roth GmbH + Co. KG) as emulsifier, with Nile Red (Carl Roth GmbH + Co. KG) employed to stain the oil phase. Polyvinyl alcohol (Mowiol, Carl Roth GmbH + Co. KG) was used for sample fixation, and FSC 22 Frozen Section Medium (Leica Biosystems GmbH, Nussloch, Germany) for sectioning prior to analysis. Calcium chloride ($CaCl_2{\cdot}2H_2O$, Carl Roth GmbH + Co. KG) was applied to induce alginate gelation. The food colorant E 131 (Indigo Carmine, Schumann & Sohn GmbH, Karlsruhe, Germany) was used to color the alginate solution during extrusion.

2.2. Binder preparation

The binder formulations were prepared with rapeseed oil concentrations of 0, 10, and 20 wt% relative to the total binder mass for the extrusion trials as well as for gelation of binder samples as standalone gels. In the binder intended for extrusion trials, the rapeseed oil was additionally stained with Nile Red at a concentration of around 0.00002 wt% for analysis via confocal laser scanning microscopy (CSLM).

For the oil-containing formulations, Tween 20 (5 wt% relative to the total binder) was first dissolved in water. A pre-emulsion was subsequently formed using an Ultra-Turrax (T25 digital, IKA-Werke GmbH & Co. KG, Germany) in a 500 ml beaker at 5200 rpm for 5 min. To obtain a fine emulsion, this mixture was further processed in a high-pressure homogenizer (Shear-Jet HL60 V2, Dyhydromatics LLC, USA) in a

single-pass configuration at 345 bar using a Y-unit. In the final step, sodium alginate was incorporated. For the 10 and 20 wt% oil formulations, alginate was added to the emulsion, whereas for the oil-free control, it was added to water. In all formulations the alginate concentration relative to the water phase was 2.6 wt%. The compositions of the binder formuations are summarized in Table A1. All formulations were subsequently mixed using an Ultra-Turrax T25 digital high-speed homogenizer in 500 ml beakers at 8000 rpm for 10 min to ensure homogeneous distribution of the alginate.

2.3. Extrusion trials

For the extrusion trials, a co-rotating twin-screw extruder (Process 16, Thermo Fisher Scientific GmbH, Karlsruhe, Germany) was used. The extrusion adapter, equipped with a pressure sensor, was followed by the bi-stream breaker plate system and a cooling die with a length of 320 mm. The bi-stream breaker plate system used in this work represented a scaled-up version of the system previously described by Pernice et al. (Pernice et al. (manuscript under review)). It comprised a plate carrier housing a first breaker plate (plate 1) for distributing the protein-mass, and a second plate (plate 2) for introducing and distributing the binder as illustrated in Fig. A13. Fig. 1 shows plate 2, illustrating the hole and channel arrangement relative to the cooling die flow area (28 mm in width and 6 mm in height). Binder distribution channels (light grey) guided the binder to predefined positions between the protein holes (red, 1 mm in diameter), while dedicated binder holes (blue, 0.5 mm in diameter) enabled its discharge into the downstream cooling die, the flow area of which is indicated in dark grey.

In all trials, a constant screw speed of 100 rpm was applied using a manufacturer-recommended standard high-moisture screw configuration. To achieve predefined protein-mass temperatures of 100, 120 and 140 °C, the first four segments of the screw section were set to 30, 50, 70 and 90 °C, respectively, while the subsequent segment temperatures, including the adapter set temperature, were adjusted individually for each operating condition. The cooling die temperature was maintained at 50 °C using a recirculating thermostat (Glacier G50, Thermo Fisher Scientific, Karlsruhe, Germany). Samples were vacuum-sealed directly after extrusion and frozen in a static freezer.

The protein-mass processed in the extruder consisted of 0.78 kg h^{-1} of SPI, dosed gravimetrically using a twin-screw feeder (DDSR20, Brabender Technologie GmbH, Duisburg, Germany), and 1.22 kg h^{-1} of a salt solution containing 1.7 wt% $CaCl_2$, supplied via a peristaltic pump (Masterflex L/S, Cole-Parmer, Vernon Hills, IL, USA). The binder was introduced into the breaker plate using an eccentric screw pump (3VHD12, ViscoTec Pumpen-und Dosiertechnik GmbH, Töging a. Inn, Germany) at flow rates of 0.08, 0.15, and 0.3 kg/h. With a density of 1010 kg m^{-3} for the alginate solution, these flow rates correspond to 4, 7, and 13 wt% of the final extrudate.

2.4. Rheological measurements

Rheological measurements were performed to characterize the protein-mass regarding the influence of a varied $CaCl_2$ content and temperature on the complex modulus. Evaporation of water could be suppressed performing the measurements under pressure by utilizing a closed cavity rheometer (CCR) (RPA Elite, TA Instruments Inc., New Castle, DE, USA). Prior to the measurements, aqueous $CaCl_2$ solutions were prepared and subsequently mixed with SPI to achieve a constant water-to-SPI ratio of 56 to 44, with $CaCl_2$ concentrations of 0, 1, and 2 wt % in the final mixtures. For protein hydration, the mixtures were vacuum-sealed and incubated at 4 °C for a minimum of 12 h. The temperature-dependent data were obtained via amplitude sweep tests conducted at a constant frequency of 5 Hz over a deformation range of 1–200 %. The reported data were collected at a strain amplitude of 4 %, ensuring that all measurements remained within the linear viscoelastic regime.

2.5. Mechanical analysis

2.5.1. Cutting test and inference of anisotropy

For the cutting tests, a modified method based on Osen et al. and Chen et al. was applied (F. L. Chen et al., 2010; Osen et al., 2014). Prior to testing, extrudates were thawed and cut to a length of 28 mm to obtain a uniform, square cross-section in top view. Measurements were performed using a ZwickiLine Z2.5 TX (ZwickRoell, Ulm, Germany) equipped with a 3 mm thick aluminium blade featuring a bevel angle of 33.4°. The samples were subsequently cut at a constant speed of 2 mm s^{-1}, with the blade oriented both orthogonal and parallel to the extrusion direction up to a deformation of 85 %, with six replicates performed for each orientation. Maximum forces of both testing directions were evaluated ($F_{max,\ orthogonal}$ and $F_{max,\ parallel}$). The anisotropy index (*AI*) was then calculated as the ratio of both quantities according to Equation (1):

$$AI = \frac{F_{max,orthogonal}}{F_{max,parallel}} \quad \text{Equation 1}$$

2.5.2. TPA and derivation of chewiness

The measurements were performed using a rheometer (HAAKE

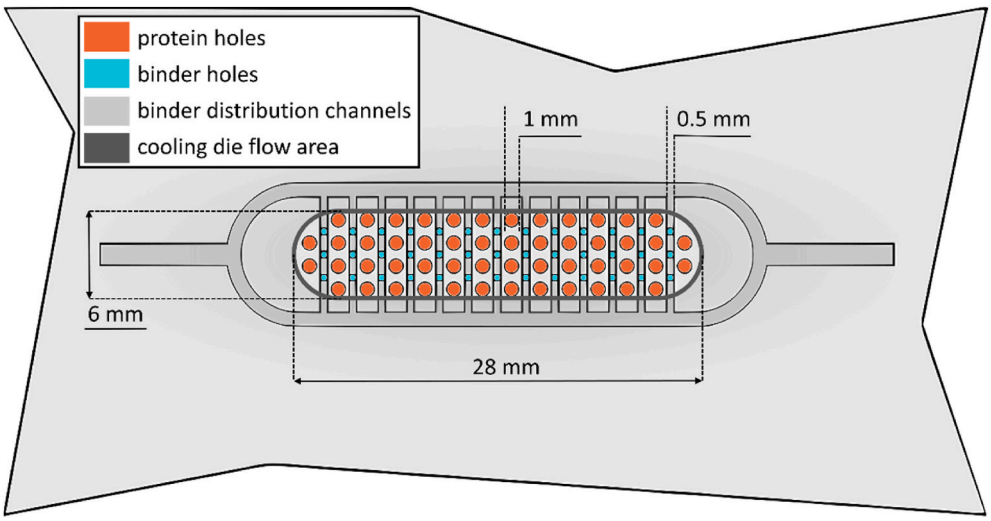

Fig. 1. Schematic illustration of plate 2 in the bi-stream breaker plate system seen from the screw section side.

MARS 60 Rheometer, Thermo Scientific Inc., Karlsruhe, Germany) equipped with a parallel plate geometry, with six replicates per condition. Cylindrical samples (15 mm in diameter) were punched from the center of thawed extrudates. A double compression test was conducted at a crosshead speed of 0.25 mm/s. Each compression cycle was performed to 25 % strain relative to the sample height at the beginning of the respective compression, with a 2 s interval between the first decompression and the second compression. Chewiness was calculated according to Equation (2), where $F_{max,1}$ denotes the maximum force during the first compression. Moreover, the areas under the force-time curves for the first and second compression ($A_{c,1}$ and $A_{c,2}$) and decompression cycles ($A_{d,1}$ and $A_{d,2}$) as well as the durations of the first and second compression ($t_{c,1}$ and $t_{c,2}$) were taken into account. The applied Equation (2) is in accordance with the one described by Dunne et al. (Dunne et al., 2025).

$$Ch = F_{max,1}\frac{(A_{c,2} + A_{d,2})t_{c,2}}{(A_{c,1} + A_{d,1})t_{c,1}} \quad \text{Equation 2}$$

2.5.3. Determination of Young's modulus of standalone binder gels

Binder formulations containing 0, 10, and 20 wt% oil were gelled via external gelation. To this end, two filter papers were soaked in a pre-prepared $CaCl_2$ solution (approx. 18 wt%) for 5 min and placed in a Petri dish (10 cm in diameter). Subsequently, 40 g of each binder formulation was poured into the Petri dish and allowed to gel for 2.5 h. After this initial gelation period, the filter papers were removed and the released syneresis water was decanted. The samples were then incubated for an additional 1.5 h to ensure complete gelation.

Subsequently cylindrical samples (9 mm in diameter) were punched out. Compression trials were carried out via a rheometer (HAAKE MARS 60, Thermo Fisher Scientific GmbH, Karlsruhe, Germany) equipped with a plate–plate geometry. The compression speed was 0,5 mm/s. Young's modulus was calculated from the strain ranging from 0.1 to 0.2 using a linear fit.

2.6. Optical analysis

To investigate the samples structural properties, tear analysis, Cryo-SEM, and CLSM were applied.

2.6.1. Tearing analysis

Thawed extrudates were cut to samples of 30 mm length and the top layer of protein strands was removed from the sample. Images of the revealed structure were captured in top view. For the variation in binder flow fraction, the mean color was quantified by analyzing the images using Fiji software (Fiji (ImageJ), NIH, Bethesda, MD, USA) in the CIELAB color space. Additionally, for each extrusion condition, an individual protein strand was photographed to reveal its shape and macroscopic morphology.

2.6.2. Cryo-SEM

Cryo-SEM imaging was carried out to gain an even deeper insight on the microstructure of the extrudates. For top-view analysis along the extrusion direction the top layer of each of selective extrudates was removed with forceps. Further sample preparation involved cutting the sample into small pieces of approximately 80 x 80 × 40 mm, and gluing them onto a plane cryo transfer shuttle with a 1:1-mixture of colloidal graphite (Agar Scientifc Ltd., Rotherham, UK) and Tissue-Tek O.C.T. compound (Sakura Tissue Tek, Tokyo, Japan). For “front view” analysis the extrudate stripes were cut into thin slices with a thickness of approximately 2 mm and mounted with the cross-section on top onto the shuttle. After plunge-freezing in nitrogen slush (T = −210 °C), each sample was instantly transferred to the pre-cooled (T = −135 °C) Polar Prep 2000 cryo preparation system (Quorum Technologies, Laughton, UK) and sublimated for 15 min at −90 °C in order to remove residual ice contamination on the surface and to reveal the morphological features of protein and binder phase. After being sputter-coated with platinum in an Argon atmosphere for 30 s (10 mA current) and final transfer to the also pre-cooled cryo-stage inside the Quanta 250 FEG SEM (FEI, Brno, Czech Republic), imaging was carried out at −135 °C with an acceleration voltage of 10 kV under high vacuum ($\sim 3 \cdot 10^{-7}$ mbar). The analysis of each extrudate was carried out in duplicate and at least five fields per protein and/or alginate phase were viewed with varying magnifications from 50× up to 5 000x.

2.6.3. CLSM

Prior to analysis, thin slices (60 μm) were prepared from extrudate samples containing 20 wt% oil in the binder in top view using a cryo-microtome (Leica Biosystems GmbH, Nussloch, Germany) at −20 °C. Samples were mounted on the specimen holder using a sectioning medium.

The obtained slices were subsequently fixed on glass slides using Mowiol and covered with cover slips. The prepared samples were then analyzed using a confocal laser scanning microscope (TCS SP5, Leica Microsystems GmbH, Wetzlar, Germany) equipped with a UV laser diode with 405 nm excitation and an argon laser, of which the 516 nm excitation line was used. For the localization of the protein phase, fluorescence was detected between 400 and 500 nm, whereas the oil phase fluorescence was detected between 600 and 700 nm. With a 10× objective, z-stacks with 2.39 μm slice thickness were recorded and reconstructed into three-dimensional images using Fiji software (Fiji (ImageJ), NIH, Bethesda, MD, USA).

2.7. Statistical analysis

For statistical analysis of the presented data, a one-way ANOVA followed by Tukey's post hoc test ($p < 0.05$) was performed using OriginPro 2023 (OriginLab Corporation, Northampton, MA, USA).

3. Results and discussion

The aim of the present study is to incorporate an ionically gelled binder into protein systems to form bi- or multi-phase, complex structured extrudates. For this purpose, different weight ratios of binder to protein-mass were investigated. Additionally, binders containing varying contents of dispersed oil were examined. The samples were characterized with respect to their structure as well as their mechanical properties. Chewiness was used as a measure to describe texture. Cutting forces and the resulting *AI* were used to quantify the directional dependence of the mechanical properties. Prior to investigating the effects of varying binder flow rates and dispersed oil fractions, the protein-mass temperature was selected as a key process parameter. Based on previous findings, this parameter was identified as critical for extrusion process stability. Therefore, the study begins with an investigation of protein-mass temperature and its impact on extrusion stability and visible structure at a constant binder flow fraction.

3.1. Variation of protein-mass temperature

Fig. 2 shows extrudates in top view, with the upper row depicting samples whose surface layer was removed to expose the internal structure, and the bottom row presenting manually isolated individual protein strands. The protein-mass temperature was set to 100, 120 and 140 °C, while the binder flow fraction was kept constant at 13 wt%.

At all temperatures, individual protein strands are clearly visible and the manual separation from the extrudates was possible. At 100 and 120 °C, the extrudates display a largely homogeneous distribution of the blue-stained binder surrounding the protein strands across the entire cross-sectional width. In contrast, at 140 °C a pronounced inhomogeneity is observed, characterized by the absence of binder in the central region of the extrudate.

A possible explanation for the inhomogeneity observed at 140 °C

Fig. 2. Top-view images of the extrudates, with the top layer removed (top row) and an isolated protein strand (bottom row), showing protein-mass temperatures of 100, 120 and 140 °C. The binder flow fraction was maintained at 13 wt%, with no oil incorporated into the binder. The extrusion direction is from left to right.

may be the obstruction of binder holes and distribution channels in the radial center of plate 2 of the bi-stream breaker plate geometry by the protein-mass. One reason for the facilitated intrusion of protein-mass into these binder pathways at 140 °C compared to 100 and 120 °C could be the decreasing viscosity with increasing temperature. This rheological behavior of SPI-water systems has been extensively investigated for SPI–water systems by various authors like (Ellwanger et al., 2025; Wittek, Ellwanger, et al., 2021). However, no data are available for concentrated SPI-water systems with $CaCl_2$ added to the mixture. Therefore, additional rheological experiments were conducted to investigate the influence of varying $CaCl_2$ content on rheological behavior of the protein-mass. All extrusion trials however were conducted with the protein-mass containing 1.1 wt% $CaCl_2$.

Fig. 3 shows the complex modulus as a function of protein-mass temperature for samples containing 0, 1, and 2 wt% $CaCl_2$. Data points were derived from amplitude sweep tests. A strain of 4 % was identified within the linear viscoelastic regime and used for data evaluation. The experiments were conducted at 100, 120 and 140 °C.

The results suggest a lowered complex modulus for increased protein-mass temperature as expected. However this effect became less pronounced with raised $CaCl_2$ concentration.

The observed behavior can be attributed to enhanced protein aggregation with increasing Ca^{2+} concentration. A major contributing factor is the increased electrostatic screening of repulsive surface charges at higher ionic strengths, which diminishes intermolecular repulsion and facilitates molecular association (Müller et al., 1996).

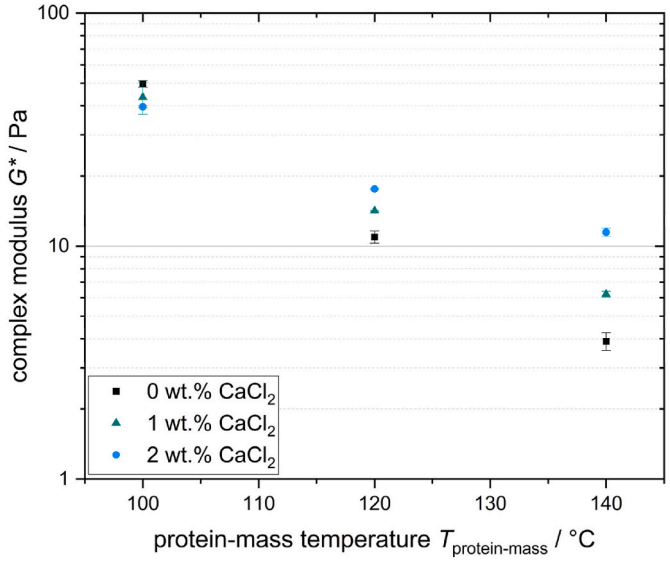

Fig. 3. Complex modulus |G*| at different protein-mass temperatures (100, 120, and 140 °C) for samples containing 0 wt% $CaCl_2$ (black squares), 1 wt% $CaCl_2$ (green triangles), and 2 wt% $CaCl_2$ (blue circles). (For interpretation of the references to color in this figure legend, the reader is referred to the Web version of this article.)

Furthermore, divalent calcium ions could promote ion bridging between negatively charged functional groups of neighboring protein molecules. Both mechanisms could contribute in the mitigation of the temperature-induced viscosity reduction. Similar calcium-mediated crosslinking mechanisms are employed in tofu manufacturing, where divalent cations induce protein gelation (Kohyama et al., 1995). In summary, the rheological experiments demonstrate a decrease in viscosity with increasing temperature, even in the presence of salt, indicating reduced flow resistance.

Consequently, the intrusion of the protein-mass into the binder holes and distribution channels is likely facilitated at elevated temperatures. It could be argued that the obstruction of the binder holes is a consequence of pressure build-up at the location of the breaker plate system, which could no longer be handled by the eccentric screw pump. However, in the extrusion trials conducted at elevated protein-mass temperatures, a lower pressure drop is expected during passage through the extruder adapter, the bi-stream breaker plate, and the cooling die. This trend is reflected in the pressure measured in the adapter during the extrusion trials (Fig. A14), which decreases from 10 bar at 100 °C to 7.5 bar at 140 °C. Moreover, even the highest measured pressure of 10 bar remains well below the manufacturer-specified maximum pressure rating of the pump (25 bar). However, it should be noted that the pressure measured in the adapter is influenced by several interacting factors and cannot be attributed solely to the rheological behavior of the protein-mass. Instead, these factors could include the gelation kinetics of the alginate-based binder and lubrication effects arising from the presence of the binder phase between the cooling die wall and the protein strands. In particular, spatial variations in binder coverage of the protein might reduce lubrication efficiency and increase frictional resistance. Furthermore, higher protein-mass temperatures at the adapter are expected to enhance heat transfer to the cooled die walls. This effect would result in a gradual convergence of viscosity and flow behavior between the protein streams of different inlet temperatures along the cooling die. The final explanation considered here can be regarded as a combination of the mechanisms discussed above. Due to the fastest cooling occurring directly at the die wall, temperature gradients across the flow cross-section may develop downstream of the breaker plate system, resulting in locally varying flow properties. The larger the temperature difference between the cooling die and the protein-mass temperature, the more pronounced the initial temperature gradient is expected to be. These inhomogeneous temperature and flow conditions, with lower-viscosity protein-mass streams flowing in the radial center, could lead to preferential obstruction of the binder holes in the radial center of the bi-stream breaker plate. According to the law of continuity, the binder flow would consequently be redirected towards the available channels in regions with a greater distance from the radial center of the flow cross-section of the breaker plate system. This effect could become self-amplifying, potentially resulting in a situation where little to no binder is distributed in the radial center of the cooling die flow cross-section. To determine whether one of the proposed mechanisms described here, or an alternative mechanism, is the predominant one, further dedicated studies are required.

Concluding, across all tested temperatures, an alginate-based binder

could be introduced via the bi-stream breaker plate and subsequently solidified in the cooling die through external ionic gelation. At 100 °C and 120 °C, the binder was predominantly distributed uniformly between the protein strands across the extrudate cross-section. Thus, the initial hypothesis is confirmed, with the qualification that at 140 °C the binder distribution was inhomogeneous across the extrudate cross-section, leaving the radial center devoid of binder. Temperature related viscosity reduction and thereby facilitated intrusion of protein-mass to the binder holes is proposed as possible explanation. For the variation of the ratio of the binder flow rate to the total extrudate flow rate, a protein-mass temperature of 120 °C was used.

3.2. Variation of the binder flow fraction

Fig. 4 shows extrudates in top view, with the upper row depicting samples with the surface layer removed to expose the internal structure, and the bottom row presenting a manually isolated individual protein strand. The binder flow fraction varied from 0 (control) to 4, 7 and 13 wt %.

At all binder flow fractions from 4 to 13 wt%, the binder exhibited a gelled state at the outflow of the cooling die which is further supported by trials on the gelation kinetics (Appendix 4.1). As expected, a distinct color change of the extrudates is visible and is quantified in Table A2. The control sample exhibits a reddish-yellowish appearance. This color shifts over green to a blue with increasing binder stream concentration. Moreover, a homogeneous distribution of the binder between the protein strands was observed for all binder flow fractions. No pronounced changes in the winding morphology of the individual protein strands were detected. Remarkably, however, the strands in the control sample appeared to exhibit sharper edges along their winding structure.

Flow instabilities of the protein strands appear to be only weakly influenced by the binder flow fraction. Even in the control sample, which served as reference, winding structures were observed. This suggests that the underlying behavior is likely dominated by effects unrelated to the binder. One explanation, previously discussed in our work (Pernice et al. (manuscript under review)), is the relaxation behavior of the protein-mass, where non-relaxed material may experience elastic recoil upon exiting the holes of the breaker plate. Another possible mechanism is gel fracture upon entering the protein holes of plate 1, as previously reported by Ellwanger et al. for similar optical phenomena observed in capillary rheology experiments (Ellwanger et al., 2025). Subsequent recombination of gel fragments in a rearranged or irregular manner after passing through the bi-stream breaker plate could explain the uneven, winding surface of the strands. The sharper edges observed in the windings can be attributed to the buffering effect of the binder during changes in strand direction. In the absence of the binder, these edges would accordingly appear more pronounced.

To evaluate the effect of the variation of the binder flow fraction variation on mechanical properties, a TPA was conducted. Chewiness was used as the evaluation parameter and calculated according to Equation (2). The results are presented in Fig. 5 for varied binder fractions from 0 to 13 wt%.

The results show a continuous, statistically significant decrease in chewiness of up to 48 % with increasing binder content. This can be explained by the higher proportion of the binder to protein strands, the mechanically weaker component of the extrudate.

Moreover, mechanical anisotropy was calculated from the cutting forces measured orthogonal and parallel to the extrusion direction according to Equation (1). The results are depicted in Fig. 6. Initial incorporation of the binder led to a significant reduction in cutting force orthogonal and perpendicular to the extrusion direction. However, further increases in the binder flow fraction did not result in additional decreases in cutting force. Accordingly, despite the relatively high standard deviations, the *AI* showed a noticeable increase upon the initial incorporation of the binder by 40 %, with no further increase observed at higher binder flow fractions.

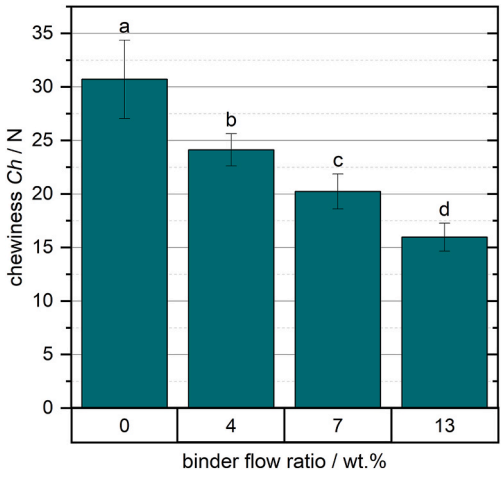

Fig. 5. Chewiness for binder flow fractions from 0 to 13 wt%. The protein-mass temperature was maintained at 120 °C, with no oil incorporated into the binder. Statistically significantly different groups are indicated by lowercase letters.

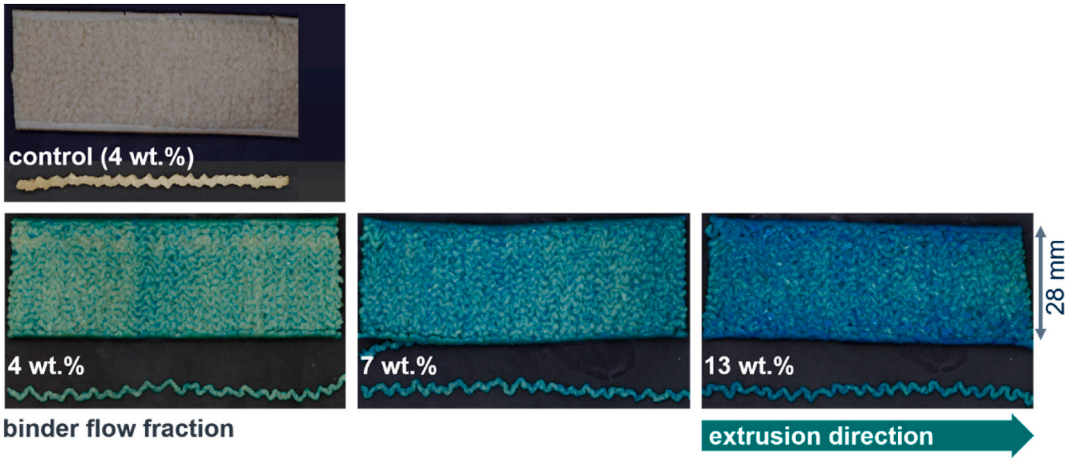

Fig. 4. Top-view images of the extrudates, with the top layer removed (top row) and an isolated protein strand (bottom row), showing binder flow fractions of 0, 4, 7, and 13 wt%. The protein-mass temperature was maintained at 120 °C, with no oil incorporated into the binder. The extrusion direction is from left to right.

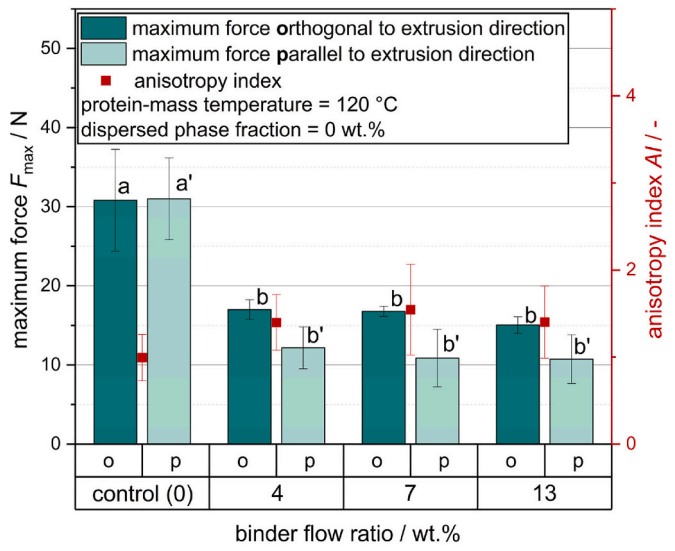

Fig. 6. Orthogonal and parallel cutting forces (F_{max}, dark and light green columns, respectively) and the resulting AI (red points) are plotted against the binder flow fraction. The binder flow fraction was varied from 0 to 13 wt%. The protein-mass temperature was maintained at 120 °C, with no oil incorporated into the binder. Statistically significantly different groupsare indicated by lowercase letters for orthogonal measurements and by lowercase letters with a prime (') for parallel measurements. (For interpretation of the references to color in this figure legend, the reader is referred to the Web version of this article.)

The reduction observed upon initial binder incorporation is attributed to an increased spatial separation of protein strands, which likely inhibits their reconnection via gel-healing mechanisms, which are known to play a critical role in the structuring of high-moisture meat analogues (van der Sman & van der Goot, 2023). The reduced inter-strand reconnection indicated here is consistent with the findings of Pernice et al., where we reported similar effects when using gelatin as a thermally gelling binder (Pernice et al. (manuscript under review)). The absence of pronounced changes at higher binder flow fractions further agrees with our recent observations, suggesting that the underlying mechanism is largely independent of the specific hydrocolloid used. Instead, the dominant factor appears to be the physical separation of protein strands by the binder, an effect determined not by the chemical nature of the binder but by its presence as a distinct spatial phase. This principle, where the major effect is governed by the spatial presence of the binder rather than its quantity, applies not only to the *AI* but also to the extrusion pressure in the adapter, for which the most pronounced pressure drop was observed between 0 and 4 wt% binder flow ratio, as shown in Fig. A15 across varying binder flow fractions. It can be concluded that a binder layer surrounding the outer protein strands reduces friction at the inner wall of the cooling die channel. The slight further decrease in pressure loss observed at higher binder flow fractions can be explained by the assumption that the lubricating effect is expected to be most pronounced in the still-liquid, ungelled state. This is attributed to the formation of a thicker binder layer between the outer protein strands and the inner wall of the cooling die, which delays gelation and therefore reduces friction over a longer distance downstream of the breaker plate system compared to lower binder flow fractions. Apart from reduced inter-strand reconnection due to spatial separation induced by initial binder incorporation, a possible explanation for the reduction of the *AI* upon binder addition is the cooling of the protein streams upon contact with the binder. The binder inlet temperature is close to room temperature and is therefore substantially cooler than the protein-mass. This might induce local cooling effects that are expected to affect protein mobility and inter-strand interactions. Furthermore, this could explain the seemingly minor influence of binder type, as similar temperature differences were also present in the study by Pernice et al. (Pernice et al. (manuscript under review)). Despite gelatin being introduced at moderately elevated temperature (50 °C), this was still well below the protein-mass temperatures.

We further propose that increasing the binder flow fraction reduces the chewiness of the extrudates, while the initial incorporation of the binder enhances structural anisotropy. Notably, further increases in the binder flow fraction are expected to have only a minor effect on anisotropy, as the protein strands are already spatially separated.

In conclusion, our hypothesis regarding the variation of the binder flow fraction can be largely confirmed. Chewiness decreased progressively with increasing binder flow fraction, while the cutting forces were primarily influenced by the initial incorporation of the alginate binder. Although no definitive conclusion can be drawn regarding the *AI* due to the high standard deviations, the initial incorporation of the binder showed a tendency towards a higher *AI* value.

3.3. *Variation of dispersed phase ratio*

Fat content is widely recognized as an important factor in food processing, particularly in meat and meat analogues, where it contributes to flavor development and perceived juiciness. In meat, lipids are primarily located within the connective tissue between muscle fiber bundles. We therefore investigated how oil dispersed in the binder phase affects the response of the resulting extrudates to mechanical stresses as indicated by chewiness and mechanical anisotropy. Addtionally, the overall structure of the resulting extrudates was visually evaluated and the impact of an oil-containing binder phase on process stability was monitored.

Fig. 7 shows extrudates in top view, with the upper row depicting samples whose surface layer was removed to expose the internal structure, and the bottom row presenting a manually isolated individual protein strand. The dispersed phase fraction was varied from 0 to 20 wt % in increments of 10 wt%.

At dispersed phase contents of 10 and 20 wt%, no additional staining of the binder was required, as the dispersed phase itself imparted a whitish coloration. For all dispersed phase fractions, the binder was distributed largely homogeneously between the protein strands across the width of the extrudate. However, slight inhomogeneities were observed, with somewhat higher binder concentrations in the peripheral regions of the extrudates.

The whitish color of the binder creates a contrast between the protein strands and the binder, resulting in a visually marbled appearance. In animal meat, marbling primarily occurs between muscle fiber bundles due to lipid deposition in the connective tissue surrounding the bundles (perimysium) (Lawrence et al., 2012). Based on the qualitative inspection of the samples shown in Fig. 7, process stability appeared to be only marginally affected by the addition of the dispersed phase, likely because the oil was incorporated within the binder and therefore did not come into direct contact with either the inner wall of the cooling die or the protein strands. These findings are supported by the extrusion pressure measured in the adapter, where no clear impact of varied oil content on the pressure measured in the adapter could be seen (Fig. A16).

Chewiness, presented in Fig. 8 for varying oil contents in the binder, decreased significantly as the oil fraction increased from 0 to 20 wt% by approximately 17 %. Although minor structural changes in binder distribution with increasing oil content were observed (Fig. 7), these effects were comparatively small. Therefore, the reduction in chewiness is more likely caused by changes in binder composition, specifically the oil fraction, rather than by alterations in spatial distribution.

To further investigate this effect, an additional experiment was conducted using pre-gelled binder material, prepared as separate standalone gels. Compression tests were performed on these materials containing 0, 10, and 20 wt% oil relative to the total binder. Fig. A19 presents the Young's modulus as a function of the oil content in the

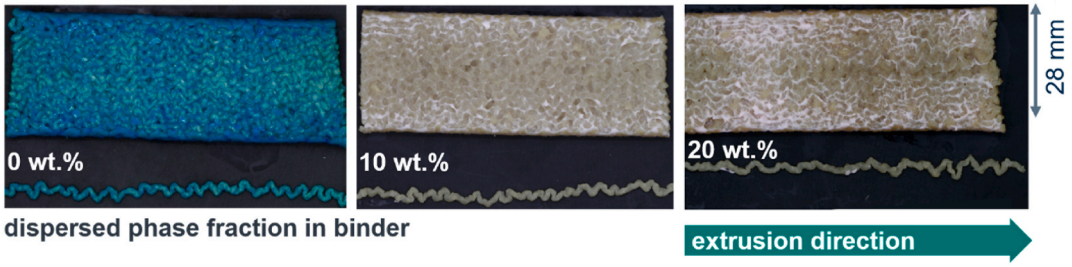

Fig. 7. Top-view images of the extrudates, with the top layer removed (top row) and an isolated protein strand (bottom row), showing dispersed phase fractions of 0, 10 and 20 wt%. The protein-mass temperature was maintained at 120 °C and the binder flow fraction at 13 wt%. The extrusion direction is from left to right.

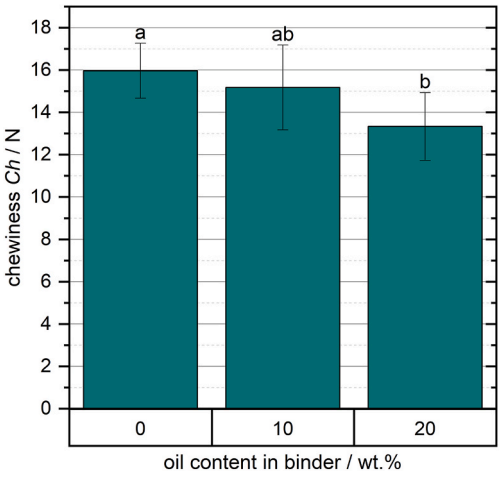

Fig. 8. Chewiness for varied oil contents in binder from 0 to 20 wt%. The protein-mass temperature was maintained at 120 °C and the binder flow fraction at 13 wt%. Statistically significant differences are indicated by lowercase letters.

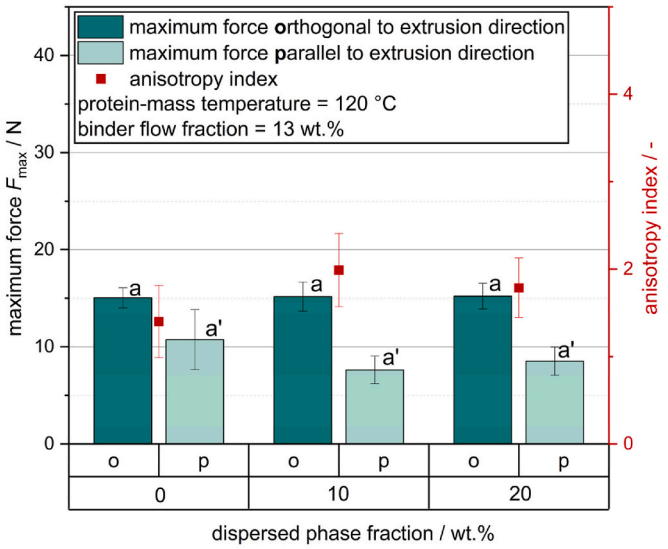

Fig. 9. Orthogonal and parallel cutting forces (F_{max}, dark and light green columns, respectively) and the resulting AI (red points) are plotted against the oil content in the binder. The dispersed phase fraction was varied from 0 to 20 wt% oil. The protein-mass temperature was maintained at 120 °C and the binder flow fraction at 13 wt%. Statistically homogeneous groups are indicated by lowercase letters for orthogonal measurements and by lowercase letters with a prime (′) for parallel measurements. (For interpretation of the references to color in this figure legend, the reader is referred to the Web version of this article.)

binder.

It is well established that droplets with non-reactive interfaces tend to reduce gel strength. Droplets embedded in this manner are often referred to as inactive fillers (Dickinson & Chen, 1999; Van Vliet, 1988). In our experiment, a consistently significant reduction of the Young's modulus with increasing oil content in the binder was observed. We therefore conclude that the rapeseed oil droplets in our binder gel, stabilized by Tween 20 and dispersed within an alginate gel matrix, behaved as inactive fillers. This conclusion is further supported by Chen et al., who reported a decrease in fracture force with increasing oil content in Tween 20-stabilized, alginate-based gels and attributed this behavior to the oil droplets acting as inactive fillers (H. Chen et al., 2021). It is important to note that the gelation conditions of the standalone gels presented in Fig. A19 substantially differ from those of the inline gelation process occurring during the extrusion experiments. Therefore, direct comparisons between the mechanical properties of the standalone gels and the extrudates are not appropriate. The results obtained from the standalone gels can only be used to compare the relative differences in Young's modulus among the different gel formulations equal gelling conditions. In conclusion, the response of the binder to mechanical stress can be modulated via the addition of a dispersed phase, thereby further affecting the chewiness of the binder-containing extrudates.

The cutting tests shown in Fig. 9 revealed no significant differences in the maximum forces parallel and orthogonal to the extrusion direction. Being calculated from these values, the *AI* shows no clear trend with varying dispersed phase fraction.

Minor variations observed in the *AI* are attributable to measurements parallel to the extrusion direction, where differences in dispersed phase content seem to have a slight effect. In contrast, when cutting orthogonal to the extrusion direction, the force-bearing elements of the material are the protein strands, whose cumulative cross-sectional area theoretically remains constant due to an unchanged binder flow fraction.

In conclusion, the addition of dispersed oil had no clear impact on mechanical anisotropy while changing chewiness towards lower levels which was attributed to the oil having a network weakening effect in the binder.

3.4. Microstructural observations

The overall properties of foods largely depend not only on their overall composition but also on the spatial distribution. To investigate the spatial distribution and microstructure of the protein matrix, alginate binder and oil within this binder, Cryo-SEM and CLSM was employed. Additional Cryo-SEM as well as SEM data sets are published as separate open-access data publication on the OpenAgrar repository (Hetzer & Pernice, 2026).

Fig. 10 presents Cryo-SEM images of control samples (0 wt% binder flow fraction) as a three-step magnification series, with top views

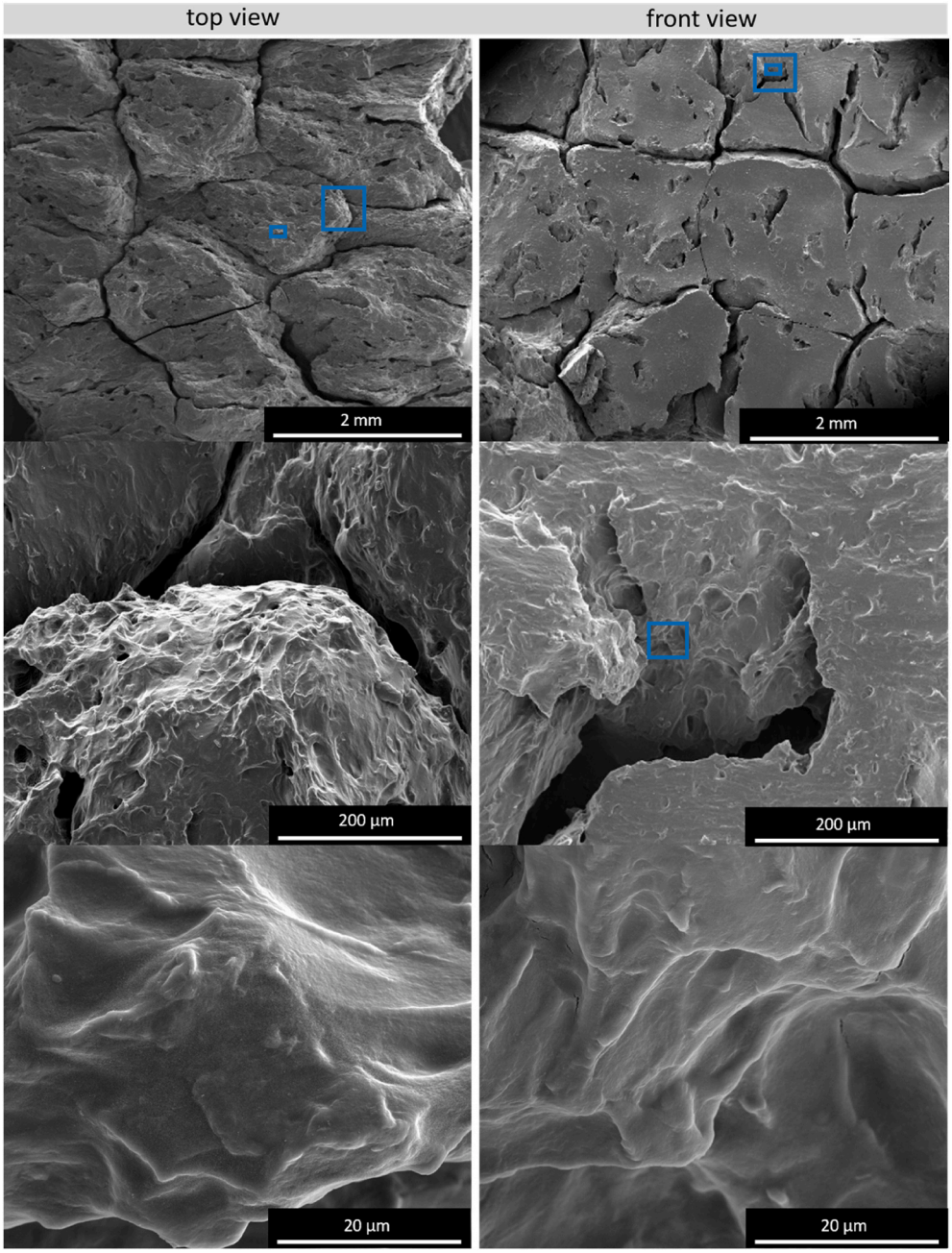

Fig. 10. Cryo-SEM images presented as a three-step magnification series of control samples (0 wt% binder flow fraction, protein-mass temperature of 120 °C), shown in top view with the upper layer of protein strands removed (left) and in front view revealed by cutting (right).

showing the upper layer of protein strands removed (left) and cross-sectional front views revealed by cutting (right). In the overview, gaps running transverse to the flow direction can be observed within the winding protein strands. These gaps may originate from water-rich regions within the protein matrix, a phenomenon previously described by Wittek et al. in the context of morphology development (Wittek, Ellwanger, et al., 2021; Wittek et al., 2021). In front view, material bridges connecting individual strands are visible, indicating partial recombination of protein strands after extrusion. Higher magnification images highlight the compact appearance of the extruded protein, consistent with observations reported in previous studies using SPI under high-moisture extrusion conditions (Deng et al., 2023; Wang et al., 2022; Zang et al., 2025).

In contrast to the control samples shown in Figs. 10 and 11 presents extrudates containing an alginate binder between the protein strands.

In the overview (top row), sheet-like layers of alginate clearly separate the protein strands. At higher magnifications focusing on the binder phase, the alginate network becomes increasingly visible, revealing structures that in the frozen state were filled with ice; this exposure is likely facilitated by sublimation during Cryo-SEM sample preparation. The transition from a thin alginate sheet to the exposed network is particularly apparent on the left side of the top-view image, where both features are present, with higher magnification in Fig. A17. At the highest magnification of the front view, a distinct directional orientation of the alginate network was observed. Although liquid nitrogen slush was used to freeze the samples prior to analysis, these orientations could be artefacts arising from the initial alignment of ice crystals during freezing or potentially from subsequent rearrangements within the frozen state.

To visualize the microstructure of extrudates containing dispersed oil

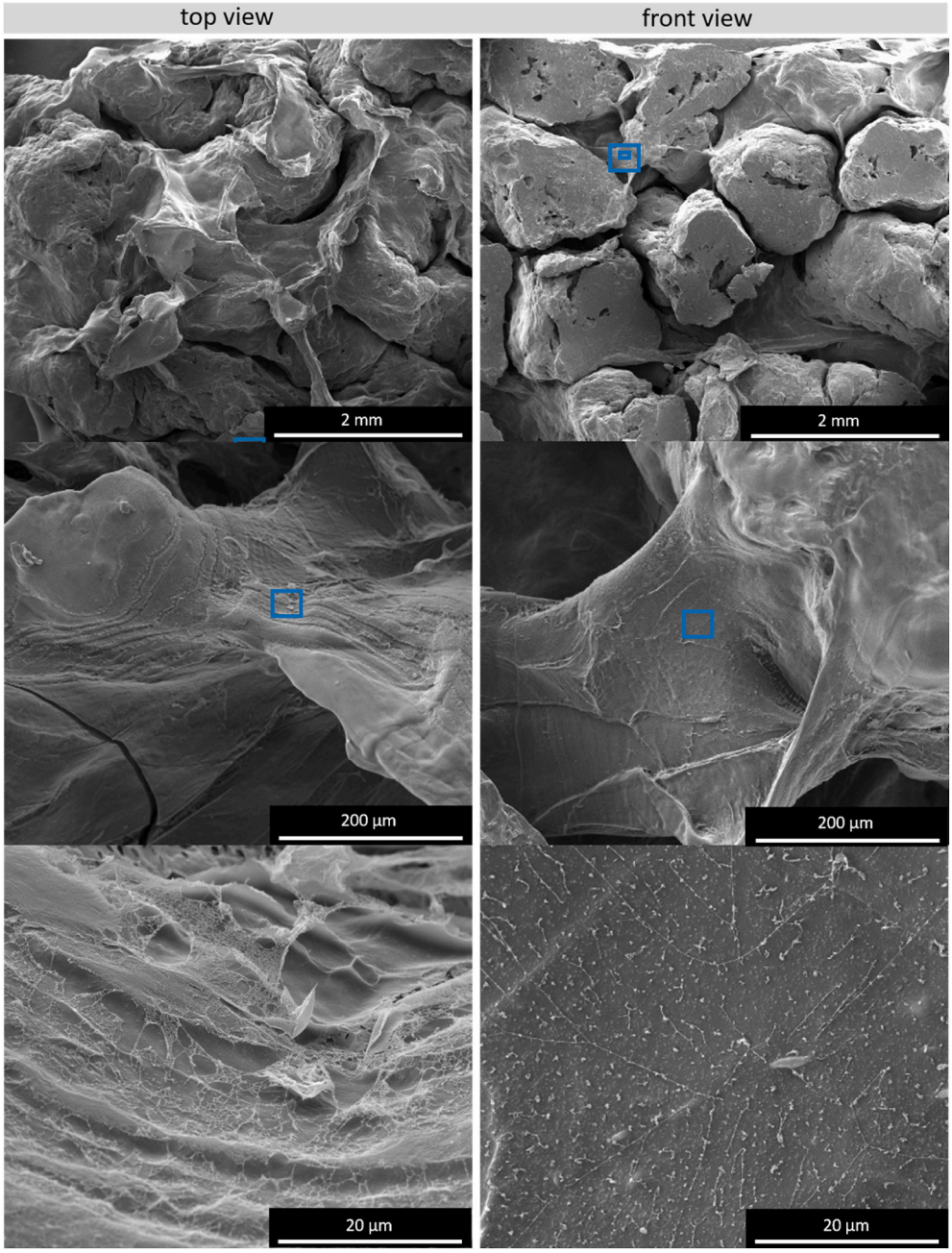

Fig. 11. Cryo-SEM images of extrudates, presented as a three-step magnification series, with the binder accounting for 13 wt% of the overall extrudate. The protein-mass temperature was 120 °C and no oil was incorporated into the binder. Samples are shown in top view with the upper layer of protein strands removed (left) and in front view revealed by cutting (right).

in an alginate-based binder, Fig. 12 presents a CLSM image (top row) of a sample with 20 wt% oil in the binder. A z-stack analysis was applied to resolve the three-dimensional distribution of the oil phase. The protein matrix is shown in green, while the stained oil phase appears in red. In the bottom row, a Cryo-SEM image provides a magnified view of the microstructural embedding of the oil within the alginate network.

The images indicate that the oil is predominantly located within the interstitial spaces between protein-rich regions. This is complementary to the findings of previous studies, such as Opaluwa et al., who reported oil encapsulation directly within the protein matrix when oil was incorporated in the screw section of the extruder (Opaluwa et al., 2024). The Cryo-SEM image confirms the encapsulation of oil droplets within the gel network. The distribution of dispersed and encapsulated oil within the alginate network, together with its spatial separation from protein-rich regions observed in the present study, could contribute to enhanced initial liquid release during consumption and, consequently, an improved perception of juiciness in high-moisture meat analogues. To evaluate this hypothesis, future studies should focus on a detailed investigation of how the composition of the binder phase influences compressive liquid release and perceived juiciness.

4. Conclusion

In this study, an alginate-based binder stream was successfully introduced into high-moisture extruded protein-mass to spatially separate strands of SPI. In order to do so, a novel bi-stream breaker plate system was employed. The breaker plate broke up the concentrated protein-mass and allowed for the dosing of binder streams at different

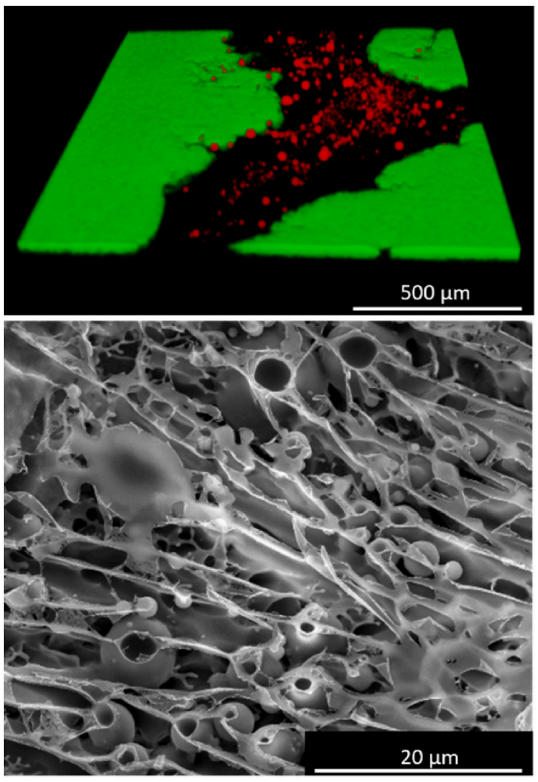

Fig. 12. Three-dimensional CLSM image (top row) of a sample prepared by cryo-sectioning and mounted on a glass slide, together with a corresponding Cryo-SEM image (bottom row) providing a magnified view of the binder gel phase of the same extrudate. The extrudate contained a binder with 20 wt% dispersed oil, with a total binder content (including oil) of 13 wt%. The protein-mass temperature was 120 °C.

flow fractions into the voids between the protein-mass streams. Gelling of the alginate binder streams was induced by diffusion of calcium ions from the protein matrix into the alginate phase. To evaluate process robustness with respect to spatial and temporal binder distribution within the extrudate, the protein-mass temperature (100, 120, and 140 °C) was varied. In addition, the binder fraction in the extrudate (0, 4, 7, and 13 wt%) and the oil content within the binder as a dispersed phase (0, 10, and 20 wt%) were systematically adjusted. Samples were characterized in terms of their optical properties (tearing Images, SEM, and CLSM) as well as their mechanical properties (chewiness and *AI*). Furthermore, rheological measurements were performed to determine the dependence of the complex modulus on temperature and $CaCl_2$ concentration in the protein-mass.

A predominantly homogeneous binder distribution between protein strands was achieved at protein-mass temperatures up to 120 °C, while processing the protein-mass to 140 °C led to strongly limited binder distribution in the radial center of the extrudate. Increasing binder incorporation reduced chewiness to a maximum difference of approximately 48 % (control vs. 13 wt% binder in extrudate), whereas mechanical anisotropy was primarily established upon initial binder addition (around 40 % increase) and remained largely unaffected by further increases. The incorporation of dispersed oil into the binder had only a minor effect on anisotropy but led to a further decrease in chewiness (17 % reduction for 20 wt% compared to 0 wt% oil), suggesting a network-weakening effect of the oil phase as it acts as an inactive filler. Microstructural analysis confirmed a spatial separation of protein and binder phases. Cryo-SEM analysis indicated the presence of oil within the alginate network, which was further confirmed by CLSM imaging.

This study demonstrates the application of a bi-stream breaker plate system for the incorporation of ionically gelling binders into conventional high-moisture extrusion processing. The ability to combine protein- and oil-rich layers into complex structures that effectively modify mechanical properties such as anisotropy and chewiness, as well as optical attributes such as visible marbling, highlights the significant potential of HEP technology. Consequently, the presented findings establish a foundation for future research on the co-extrusive creation of complex, multi-phase meat analogues. Given that the extrusion process is highly scalable and widely prevalent in the relevant industrial sectors, HEP technology moreover offers a viable pathway for the medium-term integration of next-generation meat analogues into existing production lines, as a complementary approach to conventional 3D-printing.

CRediT authorship contribution statement

Laurids Pernice: Conceptualization, Formal analysis, Funding acquisition, Investigation, Methodology, Validation, Visualization, Writing – original draft. **Luca Dennig:** Formal analysis, Investigation, Methodology, Validation. **Birgit Hetzer:** Formal analysis, Methodology, Writing – review & editing. **Eric Gottwald:** Formal analysis, Methodology, Writing – review & editing. **Ulrike S. van der Schaaf:** Resources, Supervision, Writing – review & editing. **Nico Leister:** Conceptualization, Supervision, Writing – review & editing.

Use of generative AI

During the preparation of this work the author(s) used ChatGPT (OpenAI) to support language editing, grammatical correction, and improvement of writing style. After using this tool, the author(s) reviewed and edited the content as needed and take full responsibility for the content of the published article.

Funding

L.P. gratefully acknowledges financial support by the Scholarship Program of the Deutsche Bundesstiftung Umwelt (DBU).

Declaration of competing interests

The authors declare that they have no known competing financial interests or personal relationships that could have appeared to influence the work reported in this paper.

APPENDIX

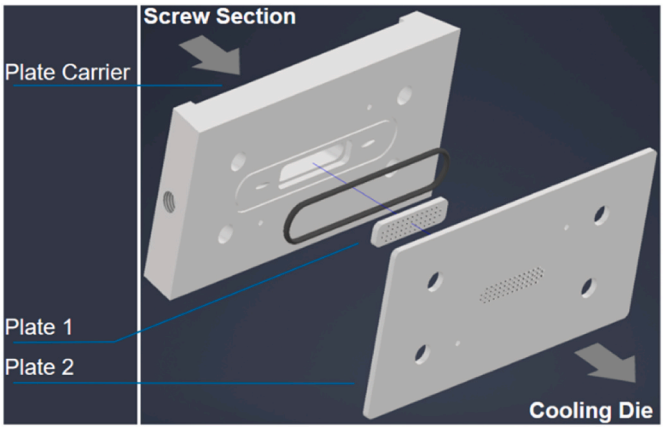

Fig. A13. Schematic illustration of the bi-stream breaker plate system, composed of a plate carrier, a sealing ring, plate 1, and plate 2, and its integration in the extrusion setup.

Table A1
Composition of the binder used in the extrusion trials and the standalone gels.

water/wt.%	oil/wt.%	tween/wt.%	alginate/wt.%
97	0	0	2,6
83	10	5	2,2
73	20	5	2,0

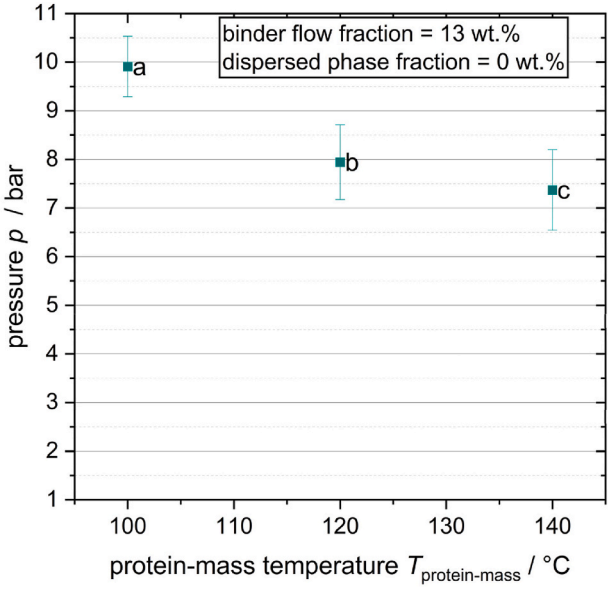

Fig. A14. Adapter pressure measured for protein-mass temperatures of 100, 120, and 140 °C, using a binder flow fraction of 13 wt %. No oil was incorporated into the binder. Lowercase letters indicate statistically significantly different groups.

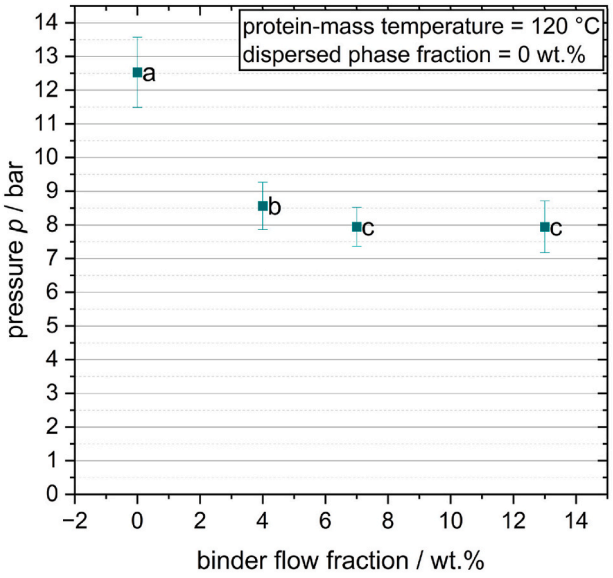

Fig. A15. Adapter pressure measured for binder flow fractions of 0, 4, 7 and 13 wt% at 120 °C protein-mass temperature. No oil was incorporated into the binder. Lowercase letters indicate statistically significantly different groups.

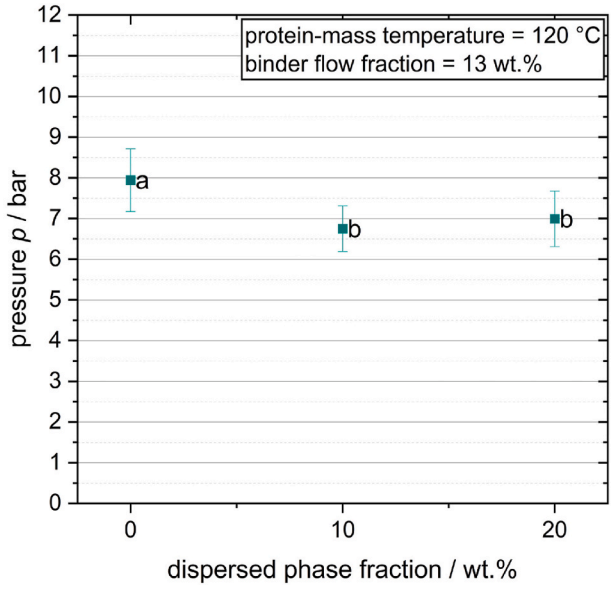

Fig. A16. Adapter pressure measured for dispersed phase fractions of 0, 10 and 20 wt% in binder at 120 °C protein-mass temperature and 13 wt% binder flow fraction. Lowercase letters indicate statistically significantly different groups.

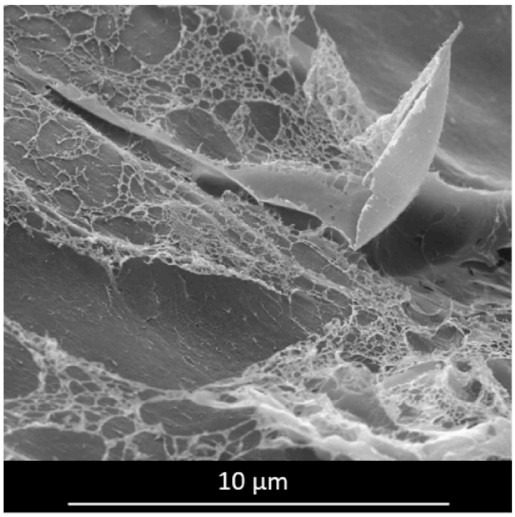

Fig. A17. Cryo-SEM image of the binder phase in an extrudate containing 13 wt% binder (relative to the total extrudate) illustrating partial ice sublimation from the alginate network. No oil was incorporated into the binder and the protein-mass temperature was 120 °C.

Table A2
Quantification of mean extrudate color on the Lab scale for binder-stream flow ratios between 0 and 13 wt%. The protein-mass temperature was 120 °C and no oil was incorporated into the binder.

	0 wt% (control)	4 wt%	7 wt%	13 wt%
L*	53.058	53.369	51.956	46.774
a*	1.882	−23.843	−25.207	−22.076
b*	4.160	5.573	−7.527	−15.085
interpretation	minor redminor yellow	green-minor yellow	green-minor blue	green-blue

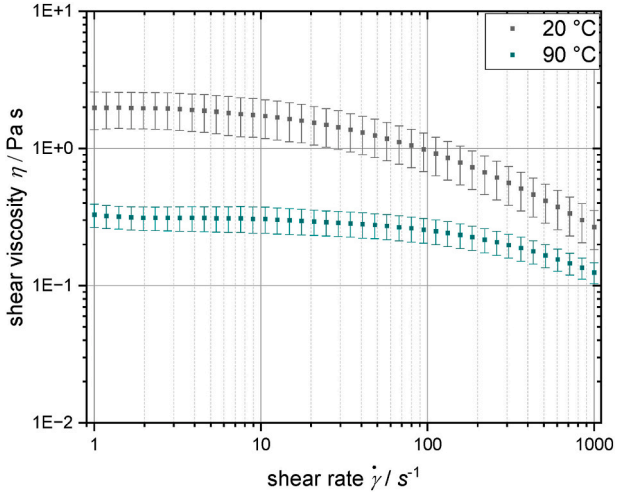

Fig. A18. Viscosity curves for 20 °C (black) and 90 °C (green) of shear rates from 1 to 1000 s^{-1}.

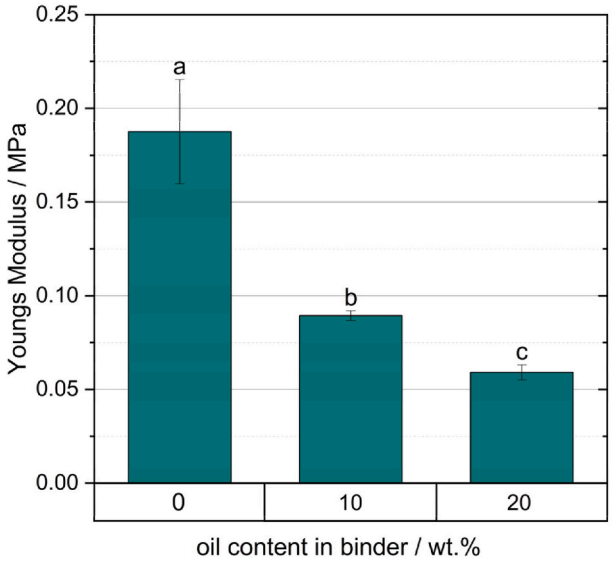

Fig. A19. Young's Modulus for varied oil contents in the standalone binder gel blocks from 0 to 20 wt%. Lowercase letters indicate statistically significantly different groups.

Gelation kinetics

Method

To estimate the gelation kinetics resulting from the diffusion of $CaCl_2$ ions from the protein strands, a separate experimental series was conducted. Extrudates of the control sample (extruded without binder at 120 °C) were cut into pieces of 70 mm. The samples were then immersed in an alginate solution containing 2.6 wt% alginate and left to gel for 3000 s (50 min) at room temperature. During this period, samples were withdrawn at eight different time points. Alginate uptake was determined gravimetrically. Using the known surface area of the extrudates, the thickness of the alginate gel layer was estimated.

Result and discussion

Fig. A20 shows the calculated gel layer thickness as a function of the gelation time with lines indicating theoretical binder layer thickness and theoretical residence time of the extruded material within the cooling die.

At a binder flow fraction of 13 wt%, the residence time of the extrudate within the 320 mm cooling die was calculated to be approximately 92 s. The theoretical binder layer thickness of 0.17 mm was derived based on the assumption that the protein strands deform into a rectangular cross-sectional shape and exhibit a linear arrangement in the axial direction. Under this assumption, the protein strands are separated by a homogeneous binder layer of constant thickness across the cooling die flow cross-section.

It can be observed that, even at room temperature, the residence time within the cooling die of approximately 92 s is sufficient to form a gel layer exceeding the theoretical thickness of the binder layer distributed within the extrudate. This estimation does not account for the fact that the binder layer within the extrudate can undergo gelation from more than one side, particularly in regions where the binder is located between two adjacent protein strands. This simplification further supports the assumption that the residence time within the cooling die is sufficient for complete gelation under the investigated process conditions.

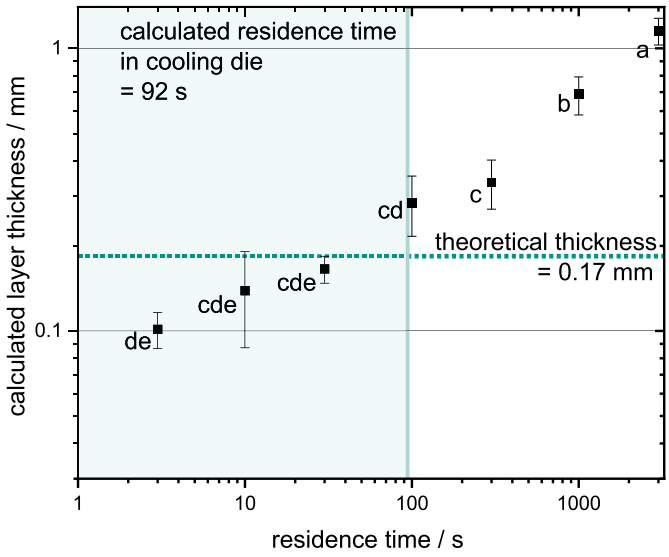

Fig. A20. Calculated alginate layer thickness at different residence times. The green dashed line indicates the theoretical binder layer thickness in extrudates with a binder flow fraction of 13 wt%, while the shaded green area represents the calculated residence time of the extrudate within the cooling die. Lowercase letters indicate statistically significantly different groups.

Data availability

Corresponding SEM and Cryo-SEM data sets are published as separate open-access data publication on the OpenAgrar repository (Hetzer & Pernice, 2026). Further data is available on request.

References

Chen, F. L., Wei, Y. M., Zhang, B., & Ojokoh, A. O. (2010). System parameters and product properties response of soybean protein extruded at wide moisture range. *Journal of Food Engineering, 96*(2), 208–213. https://doi.org/10.1016/j.jfoodeng.2009.07.014

Chen, H., Lu, Y., Yuan, F., Gao, Y., & Mao, L. (2021). Effect of interfacial compositions on the physical properties of alginate-based emulsion gels and chemical stability of co-encapsulated bioactives. *Food Hydrocolloids, 111*, Article 106389. https://doi.org/10.1016/j.foodhyd.2020.106389

Dekkers, B. L., Boom, R. M., & Van Der Goot, A. J. (2018). Structuring processes for meat analogues. *Trends in Food Science & Technology, 81*, 25–36. https://doi.org/10.1016/j.tifs.2018.08.011

Deng, Q., Wang, Z., Fu, L., He, Z., Zeng, M., Qin, F., & Chen, J. (2023). High-moisture extrusion of soy protein: Effects of insoluble dietary fiber on anisotropic extrudates. *Food Hydrocolloids, 141*(3), Article 108688. https://doi.org/10.1016/j.foodhyd.2023.108688

Dickinson, E., & Chen, J. (1999). Heat-set whey protein emulsion gels: Role of active and inactive filler particles. *Journal of Dispersion Science and Technology, 20*(1–2), 197–213. https://doi.org/10.1080/01932699908943787

Draget, K. I., Skjåk-Bræk, G., & Smidsrød, O. (1997). Alginate based new materials. *International Journal of Biological Macromolecules, 21*(1–2), 47–55. https://doi.org/10.1016/S0141-8130(97)00040-8

Draget, K. I., & Taylor, C. (2011). Chemical, physical and biological properties of alginates and their biomedical implications. *Food Hydrocolloids, 25*(2), 251–256. https://doi.org/10.1016/j.foodhyd.2009.10.007

Dunne, R. A., Darwin, E. C., Perez Medina, V. A., Levenston, M. E., St Pierre, S. R., & Kuhl, E. (2025). Texture profile analysis and rheology of plant-based and animal meat. *Food Research International, 205*, Article 115876. https://doi.org/10.1016/j.foodres.2025.115876

Ellwanger, F., Kádár, R., & Emin, M. A. (2025). Observations from capillary and closed cavity rheometry on the apparent flow behavior of a soy protein isolate dough used in meat analogues. *Applied Rheology, 35*(1), Article 20250059. https://doi.org/10.1515/arh-2025-0059

Grant, G. T., Morris, E. R., Rees, D. A., Smith, P. J. C., & Thom, D. (1973). Biological interactions between polysaccharides and divalent cations: The egg-box model. *FEBS Letters, 32*(1), 195–198. https://doi.org/10.1016/0014-5793(73)80770-7

Hecht, H., & Srebnik, S. (2016). Structural characterization of sodium alginate and calcium alginate. *Biomacromolecules, 17*(6), 2160–2167. https://doi.org/10.1021/acs.biomac.6b00378

Jeong, C., Kim, S., Lee, C., Cho, S., & Kim, S.-B. (2020). Changes in the physical properties of calcium alginate gel beads under a wide range of gelation temperature conditions. *Foods, 9*(2), 180. https://doi.org/10.3390/foods9020180

Kohyama, K., Sano, Y., & Doi, E. (1995). Rheological characteristics and gelation mechanism of tofu (soybean curd). *Journal of Agricultural and Food Chemistry, 43*(7), 1808–1812. https://doi.org/10.1021/jf00055a011

Lawrence, T. L. J., Fowler, V. R., & Novakofski, J. E. (2012). *Growth of farm animals* (3rd ed.). CABI.

Mateen, A., Mathpati, M., & Singh, G. (2023). A study on high moisture extrusion for making whole cut meat analogue: Characterization of system, process and product parameters. *Innovative Food Science & Emerging Technologies, 85*, Article 103315. https://doi.org/10.1016/j.ifset.2023.103315

McClements, D. J., & Grossmann, L. (2021). The science of plant-based foods: Constructing next-generation meat, fish, milk, and egg analogs. *Comprehensive Reviews in Food Science and Food Safety, 20*(4), 4049–4100. https://doi.org/10.1111/1541-4337.12771

Müller, R. H., Nitzsche, R., Paulke, B.-R., Mehnert, W., & Hildebrand, G. E. (Eds.). (1996). *Zetapotential und Partikelladung in der Laborpraxis: Einführung in die Theorie, praktische Meßdurchführung, Dateninterpretation*. Wiss. Verl.-Ges. CDC.

Opaluwa, C., Deskovski, S., Karbstein, H. P., & Emin, M. A. (2024). Effect of oil on the rheological properties and reaction behavior of highly concentrated wheat gluten under conditions relevant to high moisture extrusion. *Future Foods, 9*, Article 100307. https://doi.org/10.1016/j.fufo.2024.100307

Osen, R., Toelstede, S., Wild, F., Eisner, P., & Schweiggert-Weisz, U. (2014). High moisture extrusion cooking of pea protein isolates: Raw material characteristics, extruder responses, and texture properties. *Journal of Food Engineering, 127*(2–3), 67–74. https://doi.org/10.1016/j.jfoodeng.2013.11.023

Pernice, L., Röhrich, D., Gaukel, V., & Leister, N. (2025). Enhancing variability in fibrous structures via geometric modifications of breaker plates in high-moisture extrusion of meat analogues. *Journal of Food Engineering, 399*, Article 112602. https://doi.org/10.1016/j.jfoodeng.2025.112602

Pilling, M. J., & Seakins, P. W. (2007). *Reaction kinetics (Repr)*. Oxford Univ. Press.

Sha, L., & Xiong, Y. L. (2020). Plant protein-based alternatives of reconstructed meat: Science, technology, and challenges. *Trends in Food Science & Technology, 102*, 51–61. https://doi.org/10.1016/j.tifs.2020.05.022

Vallikkadan, M. S., Dhanapal, L., Dutta, S., Sivakamasundari, S. K., Moses, J. A., & Anandharamakrishnan, C. (2023). Meat alternatives: Evolution, structuring techniques, trends, and challenges. *Food Engineering Reviews, 15*(2), 329–359. https://doi.org/10.1007/s12393-023-09332-8

van der Sman, R. G. M., & van der Goot, A. J. (2023). Hypotheses concerning structuring of extruded meat analogs. *Current Research in Food Science, 6*, Article 100510. https://doi.org/10.1016/j.crfs.2023.100510

Van Vliet, T. (1988). Rheological properties of filled gels. Influence of filler matrix interaction. *Colloid and Polymer Science, 266*(6), 518–524. https://doi.org/10.1007/BF01420762

Wang, H., Van Den Berg, F. W. J., Zhang, W., Czaja, T. P., Zhang, L., Jespersen, B. M., & Lametsch, R. (2022). Differences in physicochemical properties of high-moisture extrudates prepared from soy and pea protein isolates. *Food Hydrocolloids, 128*, Article 107540. https://doi.org/10.1016/j.foodhyd.2022.107540

Wittek, P., Ellwanger, F., Karbstein, H. P., & Emin, M. A. (2021). Morphology development and flow characteristics during high moisture extrusion of a plant-based meat analogue. *Foods, 10*(8). https://doi.org/10.3390/foods10081753

Wittek, P., Zeiler, N., Karbstein, H. P., & Emin, M. A. (2021). High moisture extrusion of soy protein: Investigations on the Formation of anisotropic product structure. *Foods, 10*(1). https://doi.org/10.3390/foods10010102

Younis, K., Ashfaq, A., Ahmad, A., Anjum, Z., & Yousuf, O. (2023). A critical review focusing the effect of ingredients on the textural properties of plant-based meat products. *Journal of Texture Studies, 54*(3), 365–382. https://doi.org/10.1111/jtxs.12704

Zang, Y., Yang, R., Wang, S., Sun, C., Zhao, Y., Cao, Y., Lu, W., Zhang, Y., & Fang, Y. (2025). High-moisture soy protein extrudates with different moisture contents: Texture, structure, and in vitro digestion characteristics. *Food Research International, 210*, Article 116412. https://doi.org/10.1016/j.foodres.2025.116412

Zheng, Y., Wang, S., Sun, C., Zhao, Y., Cao, Y., Lu, W., Zhang, Y., & Fang, Y. (2024). A multihole nozzle controls recrystallization of high-moisture extruded maize starches: Effect of cooling die temperature. *Food Research International, 184*, Article 114267. https://doi.org/10.1016/j.foodres.2024.114267